Generative Adversarial Networks based Skin Lesion Segmentation

Shubham Innani^{1,*}, Prasad Dutande¹, Bhakti Baheti^{1,2}, Venu Pokuri³, Ujjwal Baid^{1,2}, Sanjay Talbar¹, and Sharath Chandra Guntuku³

ABSTRACT

Skin cancer is a serious condition that requires accurate identification and treatment. One way to assist clinicians in this task is by using computer-aided diagnosis (CAD) tools that can automatically segment skin lesions from dermoscopic images. To this end, a new adversarial learning-based framework called EGAN has been developed. This framework uses an unsupervised generative network to generate accurate lesion masks. It consists of a generator module with a top-down squeeze excitation-based compound scaled path and an asymmetric lateral connection-based bottom-up path, and a discriminator module that distinguishes between original and synthetic masks. Additionally, a morphology-based smoothing loss is implemented to encourage the network to create smooth semantic boundaries of lesions. The framework is evaluated on the International Skin Imaging Collaboration (ISIC) Lesion Dataset 2018 and outperforms the current state-of-the-art skin lesion segmentation approaches with a Dice coefficient, Jaccard similarity, and Accuracy of 90.1%, 83.6%, and 94.5%, respectively. This represents a 2% increase in Dice Coefficient, 1% increase in Jaccard Index, and 1% increase in Accuracy.

Introduction

Skin cancer is responsible for approximately 91,000 deaths each year¹. Early detection and regular monitoring are crucial in reducing skin cancer mortality rates and ensuring accurate treatment planning to improve the quality of diagnosis². A common detection method involves a dermatologist examining skin images to identify ambiguous clinical patterns of lesions that are often not visible to the naked eye. Dermoscopy, a widely used tool, helps dermatologists differentiate between malignant and benign lesions by eliminating surface reflections on the skin, thereby improving the accuracy of skin cancer diagnosis³.

Skin lesion segmentation, which is a method to differentiate foreground lesions from the background, has attracted researchers for over a decade due to its high clinical applicability and demanding nature. Computer-aided diagnostic algorithms for automated skin lesion segmentation could aid clinicians in precise treatment and diagnosis, strategic planning, and cost reduction. However, automated skin lesion segmentation is challenging due to notable discrepancies⁶, such as (i) extensive diversity in shape, texture, color, geographical conditions, and fuzzy boundaries, (ii) the presence of artifacts such as hairs, blood vessels, and veins, and (iii) poor contrast between skin and cancer lesions, as shown in Figure 1.

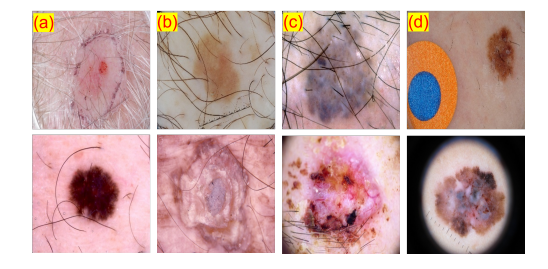


Figure 1. Challenges of dermoscopic images in skin lesion segmentation (first row): a) minor variation in the lesion and skin colour, b) low contrast between wound and skin, c) occlusion in lesions like hairs, and d) artifacts from image acquisition. Second row includes few miscellaneous examples from the dataset.

¹Center of Excellence in Signal and Image Processing, Shri Guru Gobind Singhji Institute of Engineering and Technology, Nanded, Maharashtra, India

²Center for Biomedical Image Computing and Analytics, University of Pennsylvania, Philadelphia, United States

³Department of Computer and Information Science, University of Pennsylvania, Philadelphia, United States

^{*}Corresponding Author (shubham.innani@gmail.com)

Table 1. Related Literatures	s for Skin Lesion with	CNN and GAN based approaches
-------------------------------------	------------------------	------------------------------

Reference	Summary	Model
Saliency Maps ⁴	Segmentation based on Supervised Saliency Maps	Classical
UNet Segmentation ⁵	Stochastic weight averaging using UNet CN	
Deep CNN ⁶	Full Resolution Networks	CNN
BLA-Net ⁷	Accurately segment lesion boundaries	CNN
ERU ⁸	EfficientNetB4 with UNet based encoder-decoder	CNN
AS-Net ⁹	Combines Spatial and channel attention for learning	CNN
Attention Network ¹⁰	Attention mechanism with high resolution feature	CNN
SEACU-Net ¹¹	Squeeze and Excitation based Attentive ConvLSTM	CNN
Conditional Random Fields ¹²	Deep Learning Approach with Pre and Post Processing	CNN
Conditional Random Fields ¹²	Deep Learning Approach with Pre and Post Processing	CNN
FAT-Net ¹³	Feature Adaptive Transformers	Transformer
DFE-Net ¹⁴	CNN and Transformer based Feature extraction	Transformer
SLT-Net ¹⁵	CSwin Transformer replaced Conv module in UNet	Transformer
cGAN ¹⁶	Conditional Generative Adversarial Network	GAN
Generative Network ¹⁷	Decisive Generator for skin lesion segmentation	GAN
DCGAN ¹⁸	Generating Synthetic Skin Images	GAN
FCA-Net ¹⁹	factorised channel attention and multi-scale features	GAN
DAGAN ²⁰	Deep Neural Network with generative Networks	GAN
UNet-SCDC GAN ²⁰	Levaring power of discriminators	GAN
SLS-Net ²¹	Lightweight device model with GAN	GAN

Researchers have made various efforts to develop pixel-level skin lesion segmentation. These efforts can be divided into two types: classical image processing and deep learning-based architectures. Deep learning-based methods can be further classified into Convolutional Neural Networks (CNN) and Adversarial Learning-based Generative Networks (GAN), based on the network topology. A review of a few prior works in these categories has been summarized in Table 1. Various classical approaches have been proposed in the literature, but their performance heavily depends on post-processing, such as thresholding, clustering, and hole filling, and tuning hyperparameters, such as selecting features manually. Manually tuning these parameters can be expensive and may fail to achieve desirable results. Lately, deep learning-based approaches have surpassed several classical image processing-based approaches, mainly due to the wide availability of labeled data and computing resources. The deep convolutional neural networks (DCNN) methods have delivered a promising performance in literature for skin lesion segmentation as highlighted in Table 1.

The success of prior work in skin lesion segmentation is primarily based on supervised methods that rely on large labeled datasets to extract features related to the image's spatial characteristics and deep semantic maps. However, gathering a large dataset with finely annotated images is time-consuming, expensive, and requires the expertise of medical imaging specialists. To address this challenge, Goodfellow *et al.*²² introduced Generative Adversarial Networks (GANs), which have gained popularity in various applications, including medical image synthesis, due to the lack of widely available finely annotated data. Several recent and relevant GAN-based approaches in skin lesion analysis from the literature are listed in Table 1. In the field of computer-aided medical image analysis, there is a strong demand for unsupervised learning-based algorithms that can handle large datasets without requiring ground truth labels to address real-world problems. This area of research continues to attract

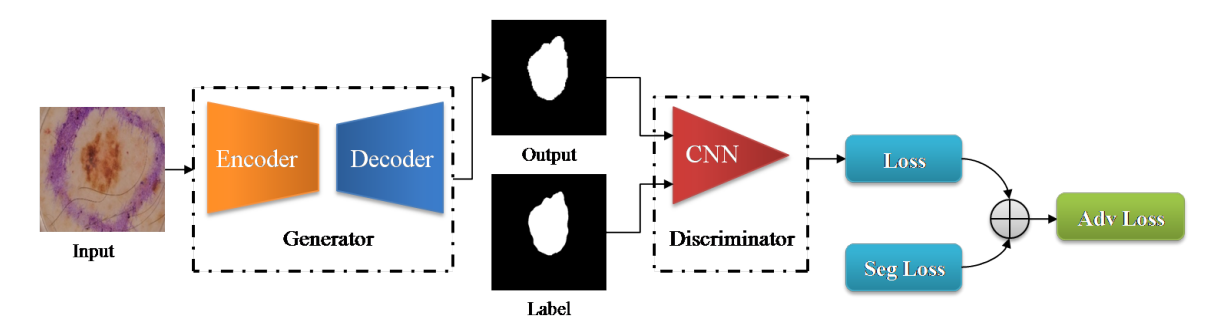
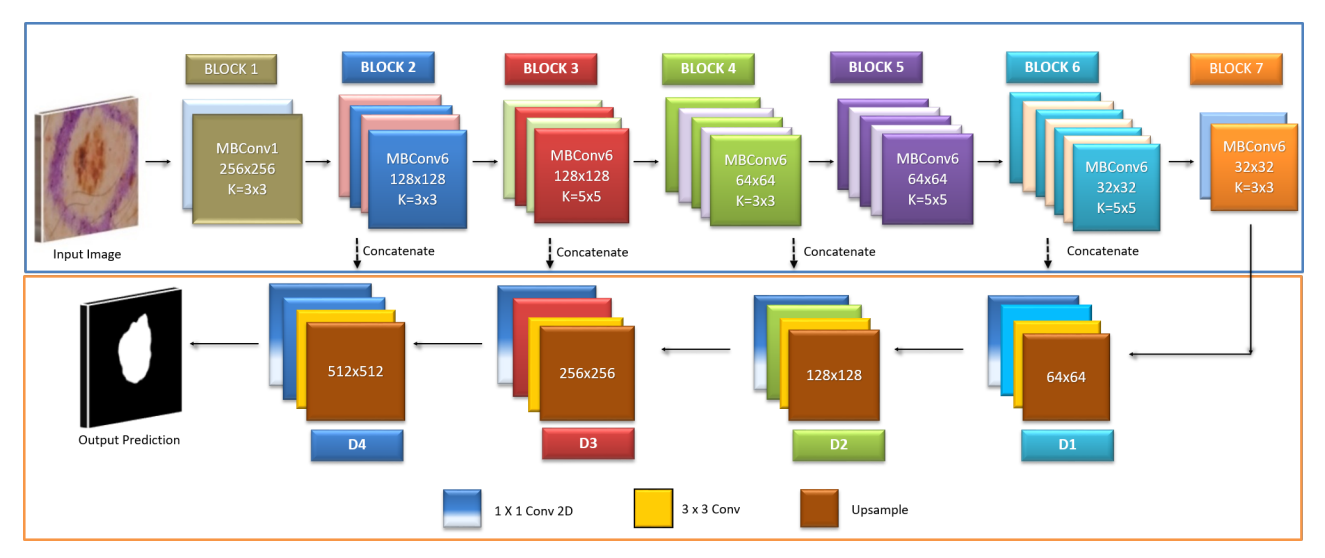
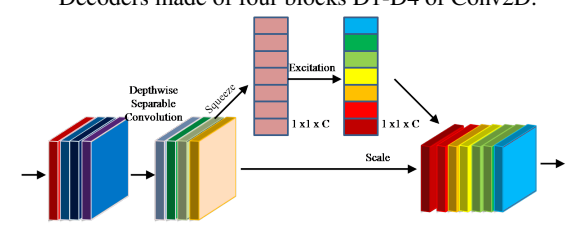


Figure 2. This figure presents a flowchart of the proposed framework. The generator module is an encoder-decoder network. The discriminator classifies the segmentation result as real or fake.



(a) Encoder has seven blocks and asymmetric concatenation to the decoder with lateral connections. Decoders made of four blocks D1-D4 of Conv2D.



(b) MBConv Block of the Encoder

Figure 3. The architecture of the proposed generator in the EGAN architecture.

multiple researchers as they seek to develop precise and high-performing networks with minimal or no labeled data.

In our work, we address the challenges of lesion segmentation by utilizing generative adversarial networks (GANs)²², which can generate accurate segmentation masks with minimal or no supervision. GANs work by training a generator and discriminator to compete against each other, where the generator tries to create realistic images and the discriminator tries to differentiate between real and generated images. However, designing an effective GAN for segmentation is not easy, as the performance is highly dependent on the architecture and loss function. In our study, we aim to optimize all three components (generator, discriminator, and loss function) to achieve better segmentation results. We believe that the choice of loss function is critical for the success of any deep learning architecture, and our approach takes this into account²³.

We propose two GAN frameworks for skin lesion segmentation. The first is EGAN, which focuses on precision and learns in an unsupervised manner, making it data-efficient. It uses an encoder-decoder based generator, patchGAN²⁴ based discriminator, and smoothing-based loss function. The generator architecture is built using a squeeze and excitation-based compound scaled encoder and lateral connection-based asymmetric decoder. This architecture captures dense features to generate fine-grained segmentation maps, and the discriminator distinguishes between synthetic and original labels. We also introduce a novel morphological-based smoothing loss function to capture fuzzy boundaries more effectively.

Although deep learning methods provide high precision for lesion segmentation, they are computationally slow, making them impractical for real-world applications with limited resources like dermatoscopy machines. This presents a challenge until high-resource devices become available to dermatologists. To address this issue, there are various devices like MoleScope II, DermLite, and HandyScope that have been developed for lesion analysis and support low computational resources. These devices use a special lens with a smartphone. To create a more practical model for real-time applications, we propose MGAN, which is a lightweight unsupervised model consisting of an Inverted Residual block²⁵ with Atrous Spatial Pyramid Pooling²⁶. The aim of this model is to achieve high pinpoint segmentation in terms of Jaccard score with minimal resources. With only 2.2M parameters, the model can run at 13 frames per second, increasing the potential impact of computer vision-based approaches in day-to-day clinical practice.

Methods

In our proposed skin lesion GAN-based segmentation framework, shown in Fig. 2, there are three main components: i) the generator, which consists of an encoder to extract feature maps and a decoder to generate segmentation maps without supervision and adapt to variations in contrast and artifacts; ii) the discriminator, which distinguishes between the reference label and the segmentation output; and iii) appropriate loss functions to prevent overfitting, achieve excellent convergence, and accurately capture fuzzy lesion boundaries.

Dataset

The proposed segmentation approach was evaluated using the ISIC 2018 dataset, which is a standard dataset for skin lesion analysis. This dataset contains 2594 images with corresponding ground truth, of which 20% (approximately 514 images) were used for validation. The images in the dataset vary in size and aspect ratio and contain lesions with different appearances in various skin areas. Some sample images from the dataset are shown in Fig. 1. To ensure a fair evaluation, the results on the test set were uploaded to the online server of the ISIC 2018²⁷ portal.

Generative Adversarial Network

Goodfellow *et al.*²² first introduced Generative adversarial networks (GAN) to generate synthetic data. Labelling clinical information is a tricky and time-consuming task requiring a specialist. Several medical imaging applications lack adequately annotated data. Inspired by this, the proposed work leverages unsupervised GAN for skin lesion segmentation. To begin with the methodology, we first briefly discuss generator and discriminator concepts. An adversarial network comprises a generator (G) and a discriminator (D). The generator maps a random vector γ from source domain space α to generate the desired output in the target domain β and tries to fool the discriminator. D learns to classify whether β is real (reference ground truth) or fake (generated by (G)). The generator's distribution p_G learns over α data, input noise distribution is defined as $P_{\gamma}(\gamma)$, which maps data space as (G)(γ ; θ_G), where differentiable function (G) has parameters θ_G . (D)(α) is the probability distribution of α from the data instead of p_G .

The adversarial training is carried out by following equation 22 which is minmax game between G and D:

$$\min_{G} \max_{D} V(D, G) = E_{\alpha \sim P_{data}(\alpha)}[log D_{\theta_D}(\alpha)] \\
+ E_{\gamma \sim P_{\gamma}(\gamma)}[log (1 - log D_{\theta_D}(G_{\theta_G}(\gamma)))]$$
(1)

where V is function of Discriminator (D), Generator (G), γ is from a input noise distribution $P_{\gamma}(\gamma)$, true samples are from $P_{data}(\alpha)$ and θ_G are generator parameters and θ_D are discriminator parameters.

Segmentation Framework

Generally, Segmentation frameworks consist of encoder-decoder-based architecture. The encoder module is the block for feature extraction to capture spatial information within the image. It reduces the spatial size, i.e. the dimension of the input image and decreases feature map resolution to catch significant level features. The decoder recuperates the spatial data by upsampling the feature map extracted by layers of the encoder and providing the output segmentation map. We propose to modify the architecture design of the encoder-decoder to capture the dense feature map rather than the traditional encoder and change the decoder appropriately, as shown in Fig. 3. Including squeeze and excitation-based compound scaled encoders significantly improves efficiency in terms of results.

Design of Encoder

Advancement of CNN designs is dependent on the accessibility of infrastructure and, afterward, the scaling of the model in terms of width (w), depth (d) or resolution (r) of the network to accomplish further significant improvement in performance when there is an expansion in the availability of resources. Instead of doing this scaling manually and arbitrarily, Tan $et\ al.^{28}$ proposed a novel systematic and automatic scaling approach by introducing a compound coefficient. The novel technique of compound coefficient ϕ to efficiently scale the network's depth, width, and resolution with a proper arrangement of scaling factors is per the following equation:

$$w: Network \ width = \beta^{\phi}$$

$$d: Network \ depth = \alpha^{\phi}$$

$$r: Input \ Resolution = \gamma^{\phi}$$

$$satisfying \ \alpha \times \beta^{2} \times \gamma^{2} \approx 2$$

$$also \ \alpha \geq 1 \ \beta \geq 1 \ \gamma \geq 1$$

$$(2)$$

Figure 4. The detailed MBConv block combines squeeze (shrinking feature map by global average pooling) and excitation(gating mechanism to produce weights) block with depthwise separable convolution.

The encoder is built using the above equation as proposed by Baheti *et al.*²⁹, and it consists of seven building blocks. Each basic building block for this encoder model is squeezing and excitation functions³⁰ with mobile inverted bottleneck convolution (MBConv), as shown in Fig. 4. Also, swish activation³¹ is used in each block of the encoder, which has enhanced performance.

Design of Decoder

The encoder downsamples the input image to a smaller resolution and captures contextual information. A decoder block likewise called an upsampling path, comprises many convolutional layers that progressively upsample the feature map obtained from the encoder. The conventional segmentation framework like UNet³² has symmetric encoder and decoder architectures. The proposed architecture builds upon a compound scaled squeeze & excitation-based encoder and decoder as an asymmetric network. The output features from the encoder are expanded in the decoder blocks consisting of bilinear upsampling. The low-level features from the encoder are combined with the higher-level feature maps from the decoder of respective sizes to generate a more precise segmentation output.

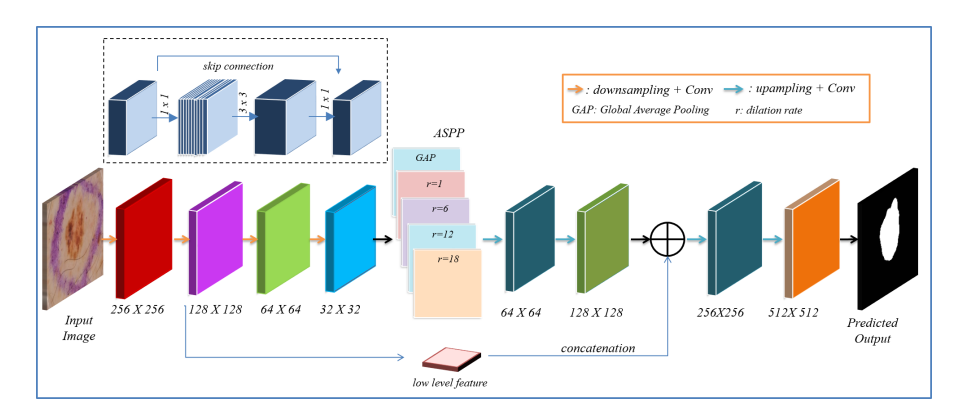


Figure 5. The architecture of the lightweight and efficient segmentation network MGAN. This architecture is based on an inverted residual network and atrous spatial pyramid pooling. The inverted residual block is shown above Encoder.

Design of lightweight segmentation framework

To develop a lightweight segmentation architecture for the generator, we leverage the power of MobileNetV2²⁵, and DeepLabV3+²⁶ consisting of atrous spatial pyramid pooling module (ASPP) as shown in Fig. 5. MobileNetV2 is built using depthwise separable convolution and inverted residual blocks as the basic building module, as shown in Fig. 5 above the encoder. MobileNetV2 is modified such that the output stride, i.e., the ratio of the input image to the output image, is 8. It has fewer computations and parameters and is thus suitable for real-time applications. The ASPP block has a variety of dilation rates, i.e., 1, 6, 12, and 18, to generate multi-scale feature maps and further integrate by concatenation. This feature map is upsampled and integrated with a low-level intermediate feature map from the contracting path, i.e., encoder, to generate fine-grained segmentation output. The feature extraction consisted of blocks of inverted residual blocks, as shown in Fig. 5. The stride of the latter blocks is set as one. Images of size $512 \times 512 \times 3$ are fed as input to MGAN architecture.

Discriminator

In our architecture, we have a generator and a discriminator. The discriminator is responsible for supervising the generator to produce precise masks that match the original ground truth. To achieve this, we have implemented a patchGAN-based approach, which classifies each $m \times n$ mask as equivalent to the ground truth. The discriminator consists of five Conv2D layers with a kernel size of 4×4 and a stride of 2×2 , with 64, 128, 256, 512, and 1 feature maps in each layer. LeakyReLU activation with an alpha value of 0.2 is used in each Conv2D layer, with the last layer using sigmoid activation. The patch-based discriminator has an output size $(m \times n)$ of 16×16 , where one pixel is linked to a patch of input probability maps with a size of 94×94 . The discriminator classifies each patch as either fake or real. This learning strategy enforces the predicted label to be similar to the ground truth. The number of parameters is the same as proposed in patchGAN²⁴.

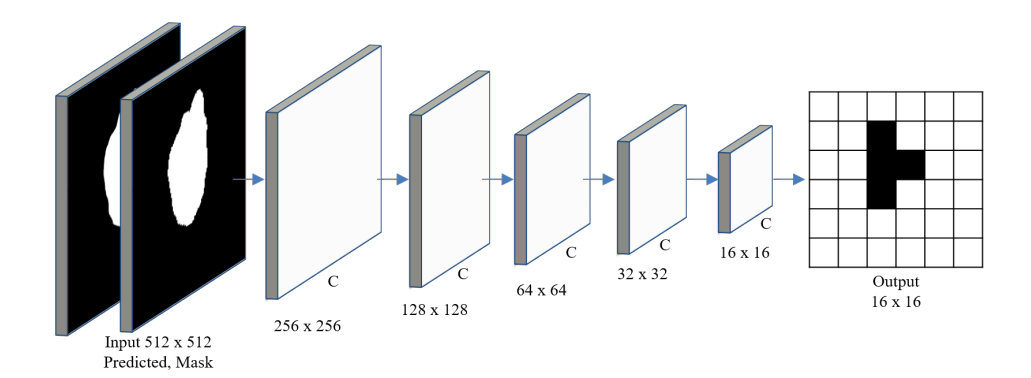


Figure 6. The discriminator architecture has a convolutional layer (C) kernel size of 4×4 and stride of 2×2 .

We practice the following adversarial technique for each generated label to align with the ground truth labels. A min-max two-step game alternatively renews the generator and discriminator network with adversarial learning. The discriminator function is given by :

$$L_D(x,y) = -\sum_{x,y} \gamma log(D(I_S)) + (1 - \gamma)log(1 - D(I_T))$$
(3)

where x, y are the pixel locations of the input, $D(I_S)$ is the Discriminator function of Source Domain Images(I_S), i.e., Label Image, $D(I_T)$ is Discriminator function of Target Domain Images (I_T), i.e., Predicted Image and γ is the probability of the predicted pixel, $\gamma = 1$ when prediction is from ground truth, i.e., source domain, and $\gamma = 0$ when prediction is from generator segmented mask, i.e., target domain.

Loss Function

We implement smoothing loss based on morphology to improve skin lesions segmentation and supervise the network that captures the lesion's smoothness and fuzzy boundaries. The network's loss function includes dice coefficient loss (L_{DL}) as well as the morphology-based smoothing loss (L_{SL}) . The dice coefficient loss assesses the cross-over between the ground truth and prediction and is given by the condition as:

Table 2. Results of CNN and GAN based approaches on ISIC 2018 test dataset. * indicates model is trained by author. - indicates data not available in literature

Approach	Network	Dice Coefficient	Accuracy	Jaccard Index	Sensitivity	Specificity
UNet*32	CNN	71.53	80.7	60.58	85.8	87.8
DeepLabV3+*33	CNN	76.3	91.4	77.3	87.8	88.1
FPN*34	CNN	84.46	92.4	73.76	88.2	87.8
Mobile-UNet*35	CNN	83.9	91.2	71.32	90	94.1
Res-UNet*35	CNN	86.3	90.8	76.77	90.9	93.7
Eff-UNet*29	CNN	89.56	92.2	81.42	90.7	92.6
CPFNet ³⁶	CNN	89.89	96.3	82.86	89.53	96.55
ERU ⁸	CNN	88.12	94.35	80.56	90.32	96.92
FAT-Net ¹³	Transformers	89.03	96.99	82	91	95.3
SEACU-Net11	CNN	87.58	93.60	78.12	-	-
SLT-Net15	Transformer	82.85	-	71.51	-	-
AS-Net ⁹	CNN	88.07	94.66	80.51	89.92	95.72
cGAN ²⁰	GAN	83.8	90.2	74.8	89.2	92.9
DCGAN ¹⁸	GAN	85.8	91.9	74.4	89.1	95.4
FCA-Net19	GAN	88.8	93.8	77.2	94.7	92.1
DAGAN ²⁰	GAN	88.5	92.9	82.5	95.3	91.1
MGAN (Ours)	GAN	88.3	93.4	75.0	93.8	92.1
EGAN (Ours)	GAN	90.1	94.5	83.6	93.6	95.5

$$L_{DL(\widehat{v},v))} = 1 - \frac{2\sum_{i \in \omega} \widehat{v}_i \cdot v_i}{\sum_{i \in \omega} \widehat{v}_i^2 + \sum_{i \in \omega} v_i^2}$$

$$\tag{4}$$

where ω is cumulative of pixels in the input image, v, and \hat{v} are the original mask and predicted mask probability map, respectively.

The morphology-based smoothing loss strengthens the network to allow smooth predictions within the nearest neighbor area³⁷. It is pairwise interaction of binary label written as:

$$L_{SL(\widehat{y},y)} = \sum_{i \in \Omega} \sum_{j \in \mathbb{N}^1} B(i,j) \times y_i \times |\widehat{y}_i - \widehat{y}_j|$$
(5)

where:
$$B_{i,j} = \begin{cases} 1 & if \ y_i = y_j \\ 0 & otherwise \end{cases}$$

where \mathbb{N}^l is four neighbor connection of pixels. y and \hat{y} denote the ground truth and prediction probability maps, respectively. The four connected neighbor algorithm based smoothing loss encourages the surrounding area of pixel j with center pixel i to produce prediction probabilities similar to original ground-truth class ($B_{i,j} = 1$).

The combined loss function is written as:

$$L_{\widehat{\mathbf{y}},\mathbf{y}} = L_{DL}(\widehat{\mathbf{y}},\mathbf{y}) + L_{SL}(\widehat{\mathbf{y}},\mathbf{y}) \tag{6}$$

Thus, complete framework works to optimize the loss function by training the network iteratively.

Results

Implementation Details

Our proposed skin lesion segmentation framework is an end-to-end solution developed in the Tensorflow 2.0 Python library. The dataset used for performance evaluation consists of 2594 images with corresponding ground truth, of which 20% were reserved for validation. The images in the dataset vary in size and aspect ratio and feature lesions with distinct appearances located in different parts of the skin. For the segmentation task, input images were resized by the nearest neighbor approach to $512 \times 512 \times 3$. The network was trained with a batch size of 8 on a Quadro 5000 16GB Nvidia GPU and optimized using the Adam optimizer with weights initialized from pre-trained ImageNet. The learning rate was fixed at 0.001 and was reduced by a factor of 0.2 every 25 epochs. To optimize the discriminator, we used the stochastic gradient descent (SGD) algorithm with a learning rate of 0.0001, which decayed polynomially with a power of 0.9. To avoid overfitting and achieve excellent convergence, we used appropriate loss functions as described in section .

Table 3. Comparison of various Mobile Networks available in the literature. The inference is Frames per Second (FPS) on original Images with a patch size of 512×512

Method	Jaccard Index	Parameters (M)	Inference (FPS)
ENet ³⁸	72.7	0.36	27
SLSNet ²¹	78.40	2.35	16
GAN FCN ³⁹	77.80	10.2	8
MGAN	75	2.2	13

Evaluation Metrics

The evaluation of segmentation is performed with various metrics like Dice Coefficient, Jaccard Score, Accuracy, Sensitivity and Specificity which are described below:

Dice coefficient measures the overlap between label and predictions and is given as:

$$\frac{2\times TP}{2\times TP + FP + FN}$$

Jaccard Score computes the Intersection over Union (IoU) between the prediction and the ground truth as :

$$\frac{TP}{TP + FP + FN}$$

Pixel classification accuracy is calculated as:

$$\frac{TP + TN}{TP + FP + TN + FN}$$

Sensitivity estimates the level of actual positive values that are accurately recognized and given as:

$$\frac{TP}{TP + FN}$$

whereas, Specificity evaluates the percentage of negative values which are rightly identified and is obtained as:

$$\frac{TN}{FP + TN}$$

where TP: True Positive where the model correctly predicts the true class, TN: True Negative where the model correctly predicts the negative class, FP: False Positive model incorrectly predicts the positive class and FN: False Negative model incorrectly predicts the negative class.

Analysis

We implemented and analyzed the results of several CNN and GAN-based approaches for this task. Table 2 summarize the evaluation of the unseen test dataset for CNN and GAN based approaches respectively. We started the experiment with famous UNet architecture in medical image segmentation³². Since this architecture is a simple stack of convolutional layers, the original UNet could not achieve remarkable performance on ISIC 2018 dataset. We strategically carried out several experiments using deeper encoders like ResNet, MobileNet, EfficientNet, and asymmetric decoders, as shown in Fig. 3. To improve performance, concatenating low-level features is skewed rather than linking each block from the encoder. The addition of the batch normalization⁴⁰ layer after each convolutional layer also helps achieve better performance. For detailed evaluation with CNN-based methods, we also experiment with DeepLabV3+²⁶ and Feature Pyramid Network (FPN)⁴¹ decoders in combination with various encoders as described above, and the modification leads to improved performance. These results on ISIC 2018 test set from our experimentation i.e. trained by us are listed with * in Table 2.

Table 2 also lists several results from recent literature for comparison completeness. Models trained by us are submitted on an evaluation server for a fair evaluation. We then compare the results of various GAN-based approaches, as shown in Table 2. The results tabulated in Table 2 provide an insight that a well-designed generative adversarial network (GAN) improves performance contrasted with the techniques with CNNs for medical image segmentation. This is because the GANs can overcome the main challenge in this domain of sufficient labelled training data being available. The extensive experiments in Table 2 indicate that our presented approach obtains superior performance. There exist a few works of literature 742368 which report better performance compared to our results. But it is to be noted that they have created and used independent test split from ISIC training data and did not use the actual ISIC test data.

Table 4. Comparison of Dice loss and morphology based smoothing loss of EGAN on ISIC 2018 testset

Loss Function	Dice Coefficient
Dice loss	88.4
Morphology loss	90.1

Discussion

The success of Generative Adversarial Networks (GANs) in skin lesion segmentation relies on the quality of the generator, discriminator, and loss function used. To address the data-efficiency challenge, we trained our model in an unsupervised manner, allowing the generator module to effectively capture features and segment the lesion without supervision. Our patchGAN-based discriminator penalizes the overall adversarial network by differentiating between labels and predictions. We also introduced a morphological-based smoothing loss to capture fuzzy lesion boundaries, resulting in a highly discriminative GAN that considers both contextual information and segmented boundaries. We designed a lightweight generator model called MGAN, based on DeepLabV3+ and MobileNetV2, which achieves results comparable to our EGAN model in terms of Dice Coefficient with significantly fewer parameters and faster inference times. Our approach is suitable for real-time applications, making it a viable solution for cutting-edge deployment challenges. Table 3 provides a comprehensive comparison of various mobile architectures

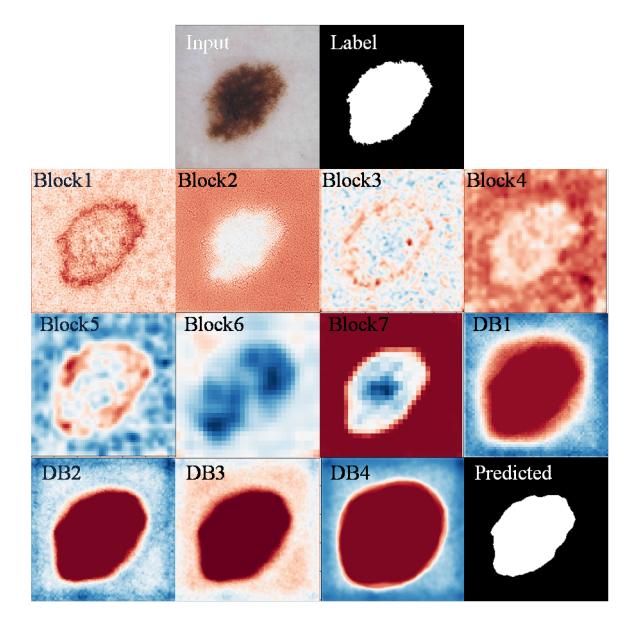


Figure 7. Visualization of the feature maps of proposed EGAN architecture.

based on the Jaccard Index, the number of parameters in a million, and inference speed on the test dataset for a patch size of 512×512 .

In skin lesion segmentation, capturing contextual information around the segmentation boundary is crucial for improving performance⁷. To achieve this, we introduce a morphology-based smoothing loss function in our GAN framework, which effectively captures smooth masks. Our proposed EGAN model achieves improved performance with a dice coefficient of 90.1% on the ISIC 2018 test dataset when trained with adversarial learning and morphology-based smoothing loss function compared to using the dice loss alone, which achieved a dice coefficient of 88.4%. Fig. 8 displays the segmentation results for visual interpretation. The proposed GAN framework also demonstrates better segmentation performance regardless of the presence of non-skin objects or artifacts in the image. To the best of our knowledge, this is the first study to present unsupervised learning-based skin lesion segmentation.

Some researchers argue that although deep neural networks can make valuable and skillful predictions, they are generally opaque, i.e., unclear how or why a particular prediction or decision is made. To address concerns about the opacity of deep neural networks, we utilized the internal structures of convolutional neural networks that work on 2D image data to investigate the data learned by our unsupervised model. We assessed and visualized the 2D filter weights of the model to explore the features learned by the model. Additionally, we investigated the activation layers of the model to understand precisely which features the model recognized for a given input image, and we displayed the results in Fig. 7 for visual understanding. We selected the output of seven blocks of the encoder (Block1-Block7) and four output feature maps from the decoder (D1-D4) for visualization as the model has numerous convolutional layers in each block of the architecture. Our proposed framework extracts discriminative features and fine-grained information for lesion segmentation, revealing the potential of our methodology.

Conclusion

This research proposes a novel unsupervised adversarial learning-based framework to capture fine-grained skin lesion segmentation. Our proposed framework includes two generative models: the performance-exclusive EGAN and the computational-exclusive MGAN, which are designed to balance performance and efficiency.. Both models incorporate a patchGAN-based discriminator to optimize the generator's decisions, and a novel smoothing loss function is introduced to capture fuzzy and varying boundaries. Our evaluation on the ISIC 2018 dataset demonstrates significantly improved performance compared to existing models in the literature. Furthermore, the proposed framework's potential can be extended to other medical imaging applications. Overall, this work contributes to the field of medical image analysis by providing a new method for accurate and efficient skin lesion segmentation.

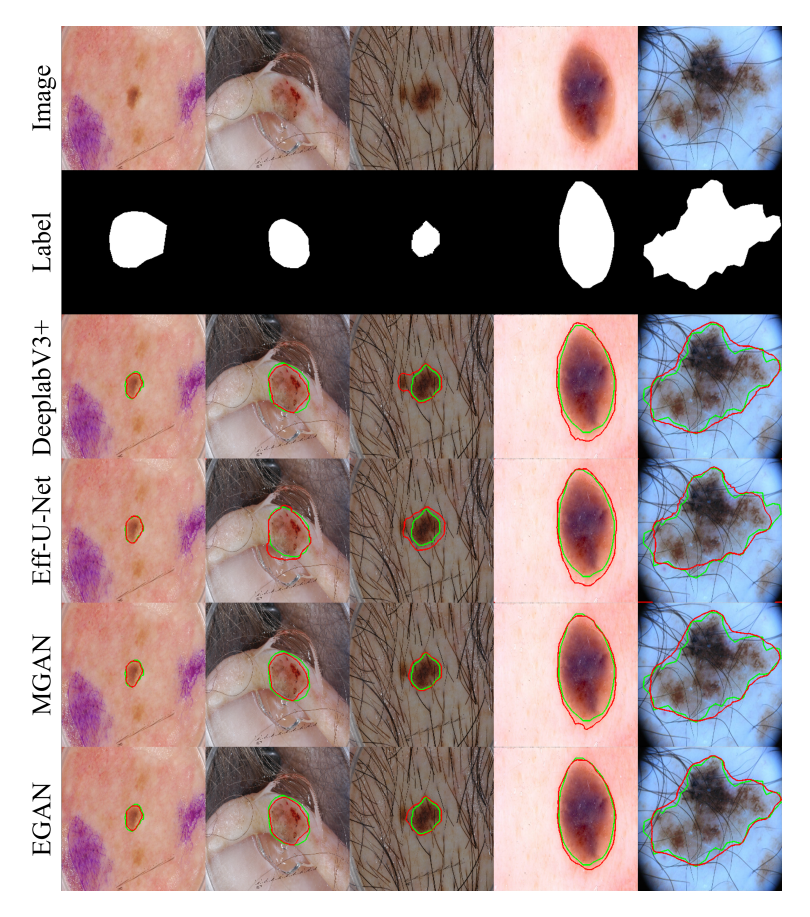


Figure 8. This figure shows the segmentation performance comparison of various CNN and GAN-based approaches. Each row serially depicts Input Image, Label, output of CNN Approaches and output of GAN Approaches MGAN and EGAN. Ground truth and segmented lesions are marked with green and red curves.

References

- **1.** Society, C. Melanoma stats, facts, and figures. https://www.aimatmelanoma.org/about-melanoma/melanoma-stats-facts-and-figures. (2018). [Online accessed on 20-February-2020].
- **2.** Rigel, D. S., Russak, J. & Friedman, R. The evolution of melanoma diagnosis: 25 years beyond the abcds. *CA: A Cancer J. for Clin.* **60**, 301–316, DOI: 10.3322/caac.20074.
- **3.** Centre, S. Dermoscopy and mole scans in perth and regional wa. https://myskincentre.com.au/service/dermoscopy/ (2018). [Online accessed on 20-February-2020].
- **4.** Jahanifar, M., Zamani Tajeddin, N., Mohammadzadeh Asl, B. & Gooya, A. Supervised saliency map driven segmentation of lesions in dermoscopic images. *IEEE J. Biomed. Heal. Informatics* **23**, 509–518, DOI: 10.1109/JBHI.2018.2839647 (2019).
- **5.** Tang, P. *et al.* Efficient skin lesion segmentation using separable-unet with stochastic weight averaging. *Comput. Methods Programs Biomed.* **178**, 289–301, DOI: https://doi.org/10.1016/j.cmpb.2019.07.005 (2019).
- 6. Al-masni, M. A., Al-antari, M. A., Choi, M.-T., Han, S.-M. & Kim, T.-S. Skin lesion segmentation in dermoscopy images via deep full resolution convolutional networks. *Comput. Methods Programs Biomed.* 162, 221–231, DOI: https://doi.org/10.1016/j.cmpb.2018.05.027 (2018).
- 7. Feng, R., Zhuo, L., Li, X., Yin, H. & Wang, Z. Bla-net:boundary learning assisted network for skin lesion segmentation. *Comput. Methods Programs Biomed.* 226, 107190, DOI: https://doi.org/10.1016/j.cmpb.2022.107190 (2022).
- **8.** Nguyen, D. K., Tran, T.-T., Nguyen, C. P. & Pham, V.-T. Skin lesion segmentation based on integrating efficientnet and residual block into u-net neural network. In *2020 5th International Conference on Green Technology and Sustainable Development (GTSD)*, 366–371, DOI: 10.1109/GTSD50082.2020.9303084 (2020).

- 9. Hu, K., Lu, J., Lee, D., Xiong, D. & Chen, Z. As-net: Attention synergy network for skin lesion segmentation. *Expert. Syst. with Appl.* 201, 117112, DOI: https://doi.org/10.1016/j.eswa.2022.117112 (2022).
- **10.** Xie, F. *et al.* Skin lesion segmentation using high-resolution convolutional neural network. *Comput. Methods Programs Biomed.* **186**, 105241, DOI: https://doi.org/10.1016/j.cmpb.2019.105241 (2020).
- 11. Jiang, X., Jiang, J., Wang, B., Yu, J. & Wang, J. Seacu-net: Attentive convlstm u-net with squeeze-and-excitation layer for skin lesion segmentation. *Comput. Methods Programs Biomed.* 225, 107076, DOI: https://doi.org/10.1016/j.cmpb.2022.107076 (2022).
- **12.** Ashraf, H., Waris, M., Ghafoor, M., Gilani, S. & Niazi, I. Melanoma segmentation using deep learning with test-time augmentations and conditional random fields. *Sci. Reports* DOI: 10.1038/s41598-022-07885-y (2022).
- **13.** Wu, H. *et al.* Fat-net: Feature adaptive transformers for automated skin lesion segmentation. *Med. Image Analysis* **76**, 102327, DOI: https://doi.org/10.1016/j.media.2021.102327 (2022).
- **14.** Fan, C., Yang, L., Lin, H. & Qiu, Y. Dfe-net: Dual-branch feature extraction network for enhanced segmentation in skin lesion. *Biomed. Signal Process. Control.* **81**, 104423, DOI: https://doi.org/10.1016/j.bspc.2022.104423 (2023).
- **15.** Feng, K., Ren, L., Wang, G., Wang, H. & Li, Y. Slt-net: A codec network for skin lesion segmentation. *Comput. Biol. Medicine* **148**, 105942, DOI: https://doi.org/10.1016/j.compbiomed.2022.105942 (2022).
- 16. Mirza, M. & Osindero, S. Conditional generative adversarial nets, DOI: 10.48550/ARXIV.1411.1784 (2014).
- 17. Izadi, S., Mirikharaji, Z., Kawahara, J. & Hamarneh, G. Generative adversarial networks to segment skin lesions. In 2018 *IEEE 15th International Symposium on Biomedical Imaging (ISBI 2018)*, 881–884, DOI: 10.1109/ISBI.2018.8363712 (2018).
- **18.** Bissoto, A., Perez, F., Valle, E. & Avila, S. Skin lesion synthesis with generative adversarial networks. In *OR 2.0 Context-Aware Operating Theaters, Computer Assisted Robotic Endoscopy, Clinical Image-Based Procedures, and Skin Image Analysis*, 294–302 (Springer International Publishing, Cham, 2018).
- **19.** Singh, V. *et al.* Fca-net: Adversarial learning for skin lesion segmentation based on multi-scale features and factorized channel attention. *IEEE Access* DOI: 10.1109/ACCESS.2019.2940418 (2019).
- **20.** Lei, B. *et al.* Skin lesion segmentation via generative adversarial networks with dual discriminators. *Med. Image Analysis* **64**, 101716, DOI: https://doi.org/10.1016/j.media.2020.101716 (2020).
- **21.** Sarker, M. M. K. *et al.* Slsnet: Skin lesion segmentation using a lightweight generative adversarial network. *Expert. Syst. with Appl.* **183**, 115433, DOI: https://doi.org/10.1016/j.eswa.2021.115433 (2021).
- 22. Goodfellow, I. et al. Generative adversarial networks. Adv. Neural Inf. Process. Syst. 3 (2014).
- **23.** Kervadec, H. *et al.* Boundary loss for highly unbalanced segmentation. In Cardoso, M. J. *et al.* (eds.) *Proceedings of The 2nd International Conference on Medical Imaging with Deep Learning*, vol. 102 of *Proceedings of Machine Learning Research*, 285–296 (PMLR, 2019).
- **24.** Isola, P., Zhu, J., Zhou, T. & Efros, A. A. Image-to-image translation with conditional adversarial networks. In *2017 IEEE Conference on Computer Vision and Pattern Recognition (CVPR)*, 5967–5976 (2017).
- **25.** Sandler, M., Howard, A., Zhu, M., Zhmoginov, A. & Chen, L. Mobilenetv2: Inverted residuals and linear bottlenecks. In 2018 IEEE/CVF Conference on Computer Vision and Pattern Recognition, 4510–4520, DOI: 10.1109/CVPR.2018.00474 (2018).
- **26.** Chen, L.-C., Zhu, Y., Papandreou, G., Schroff, F. & Adam, H. Encoder-decoder with atrous separable convolution for semantic image segmentation. In Ferrari, V., Hebert, M., Sminchisescu, C. & Weiss, Y. (eds.) *Computer Vision ECCV 2018*, 833–851 (Springer International Publishing, Cham, 2018).
- **27.** Codella, N. C. F. *et al.* Skin lesion analysis toward melanoma detection 2018: A challenge hosted by the international skin imaging collaboration (ISIC). *CoRR* **abs/1902.03368** (2019). 1902.03368.
- **28.** Tan, M. & Le, Q. V. Efficientnet: Rethinking model scaling for convolutional neural networks. *CoRR* **abs/1905.11946** (2019). 1905.11946.
- **29.** Baheti, B., Innani, S., Gajre, S. & Talbar, S. Eff-unet: A novel architecture for semantic segmentation in unstructured environment. In 2020 IEEE/CVF Conference on Computer Vision and Pattern Recognition Workshops (CVPRW), 1473–1481, DOI: 10.1109/CVPRW50498.2020.00187 (2020).
- **30.** Hu, J., Shen, L. & Sun, G. Squeeze-and-excitation networks. In 2018 IEEE/CVF Conference on Computer Vision and Pattern Recognition, 7132–7141 (2018).

- 31. Ramachandran, P., Zoph, B. & Le, Q. V. Swish: a self-gated activation function. arXiv: Neural Evol. Comput. (2017).
- **32.** Ronneberger, O., Fischer, P. & Brox, T. U-net: Convolutional networks for biomedical image segmentation. In Navab, N., Hornegger, J., Wells, W. M. & Frangi, A. F. (eds.) *Medical Image Computing and Computer-Assisted Intervention MICCAI 2015*, 234–241 (Springer International Publishing, Cham, 2015).
- **33.** Baheti, B., Innani, S., Gajre, S. & Talbar, S. Semantic scene segmentation in unstructured environment with modified deeplabv3+. *Pattern Recognit. Lett.* **138**, 223–229, DOI: https://doi.org/10.1016/j.patrec.2020.07.029 (2020).
- **34.** Innani, S., Dutande, P., Baheti, B., Talbar, S. & Baid, U. Fuse-pn: A novel architecture for anomaly pattern segmentation in aerial agricultural images. In *2021 IEEE/CVF Conference on Computer Vision and Pattern Recognition Workshops* (CVPRW), 2954–2962, DOI: 10.1109/CVPRW53098.2021.00331 (2021).
- **35.** Innani, S., Dutande, P., Baheti, B., Baid, U. & Talbar, S. Deep learning based novel cascaded approach for skin lesion analysis (2023). 2301.06226.
- **36.** Feng, S. *et al.* Cpfnet: Context pyramid fusion network for medical image segmentation. *IEEE Transactions on Med. Imaging* **39**, 3008–3018, DOI: 10.1109/TMI.2020.2983721 (2020).
- **37.** Wang, S., Yu, L., Yang, X., Fu, C.-W. & Heng, P.-A. Patch-based output space adversarial learning for joint optic disc and cup segmentation. *IEEE Transactions on Med. Imaging* **38**, 2485–2495, DOI: 10.1109/TMI.2019.2899910 (2019).
- **38.** Paszke, A., Chaurasia, A., Kim, S. & Culurciello, E. Enet: A deep neural network architecture for real-time semantic segmentation, DOI: 10.48550/ARXIV.1606.02147 (2016).
- **39.** Bi, L., Feng, D. & Kim, J. Improving automatic skin lesion segmentation using adversarial learning based data augmentation, DOI: 10.48550/ARXIV.1807.08392 (2018).
- **40.** Ioffe, S. & Szegedy, C. Batch normalization: Accelerating deep network training by reducing internal covariate shift. In *Proceedings of the 32nd International Conference on International Conference on Machine Learning Volume 37*, ICML'15, 448–456 (JMLR.org, 2015).
- **41.** Lin, T. *et al.* Feature pyramid networks for object detection. In 2017 IEEE Conference on Computer Vision and Pattern Recognition (CVPR), 936–944 (2017).
- **42.** Han, Q. *et al.* Hwa-segnet: Multi-channel skin lesion image segmentation network with hierarchical analysis and weight adjustment. *Comput. Biol. Medicine* **152**, 106343, DOI: https://doi.org/10.1016/j.compbiomed.2022.106343 (2023).

Acknowledgements

Authors are grateful to Center of Excellence, Signal and Image Processing, Shri Guru Gobind Singhji Institute of Engineering and Technology, Vishnupuri, Nanded, Maharashtra, India

Author contributions statement

S.I and P.D. conducted and analyzed the experiment, B.B. and U.B. wrote main manuscript text. V.P. helped in prepared figures. S.T. and S.C.G. guided the complete work. S.I, B.B, S.C.G. reviewed the manuscript.

Data Availability

The dataset used in this work is available in ISIC archive publicly at https://challenge.isic-archive.com/data/#2018

Code Availability

The source code is available at https://github.com/shubhaminnani/EGAN.

Competing interests

The authors declare no Competing Interest.